Structure of molten trivalent metal bromides studied by using neutron diffraction: the systems $DyBr_3$, YBr_3, $HoBr_3$ and $ErBr_3$

2000 J. Phys.: Condens. Matter 12 9539

(http://iopscience.iop.org/0953-8984/12/46/302)

J. Phys.: Condens. Matter **12** (2000) 9539–9550. Printed in the UK PII: S0953-8984(00)16556-7

Structure of molten trivalent metal bromides studied by using neutron diffraction: the systems $DyBr_3$, YBr_3, $HoBr_3$ and $ErBr_3$

Jonathan C Wasse†, Philip S Salmon‡‖ and Robert G Delaplane§

† Department of Physics and Astronomy, University College London, Gower Street, London WC1E 6BT, UK
‡ Department of Physics, University of Bath, Bath BA2 7AY, UK
§ Studsvik Neutron Research Laboratory, Uppsala University, S-61182 Nyköping, Sweden

Received 21 August 2000

Abstract. The structure of the salts MBr_3, where M^{3+} denotes Dy^{3+}, Y^{3+}, Ho^{3+} or Er^{3+}, was investigated by using neutron diffraction. On heating $DyBr_3$, YBr_3 and $HoBr_3$, a phase transition from the $FeCl_3$-type crystal structure to possibly the YCl_3-type crystal structure was observed. The liquids were studied at the total-structure-factor level and difference function methods were also applied to $DyBr_3$ and YBr_3 by assuming isomorphous structures. The melts are found to comprise distorted MBr_6^{3-} octahedra with M–Br distances comparable to the sum of the ionic radii and there is evidence for a substantial number of edge-sharing configurations. The octahedra pack to give intermediate-range ionic ordering as manifested by the appearance of a first sharp diffraction peak at 0.79(2)–0.87(2) $Å^{-1}$ which is associated with cation correlations

1. Introduction

The object of this paper is to present neutron diffraction results on the structure of the trivalent metal bromides MBr_3, where M^{3+} denotes Dy^{3+}, Y^{3+}, Ho^{3+} or Er^{3+}. Motivation for the work is provided by the paucity of information on the structure of molten trivalent metal bromides and its dependence on the ratio of the cation to the anion radius. Neutron diffraction results are available for molten $AlBr_3$ and $GaBr_3$ (Saboungi *et al* 1993) which comprise small cations and form molecular-like liquids. More recently, neutron and x-ray diffraction results have been reported for molten $LaBr_3$ (Wasse and Salmon 1999a, Okamoto and Ogawa 1999) and $CeBr_3$ (Wasse and Salmon 1999a) which comprise large cations and crystallize to form a 3-D chain-like arrangement of ions in the UCl_3-type structure (Zachariasen 1948, Taylor and Wilson 1974). By comparison, the present work focuses on systems comprising intermediate-sized cations which crystallize at room temperature to form a 2-D layered network in the $FeCl_3$-type structure (Brown *et al* 1968, Müller 1993).

Interest in trivalent metal halides stems partly from the possibility that their microscopic properties for a wide range of ion size might be accurately described using a recently developed polarizable-ion model for the interactions (Madden and Wilson 1996, Hutchinson *et al* 1999). A rich diversity in the behaviour of these systems is found; the systems adopt an increasingly 'covalent' character with decreasing cation radius. The new experimental results will enable the transferability of the polarizable-ion model from MCl_3 to MBr_3 systems to be tested

‖ Author to whom any correspondence should be addressed.

0953-8984/00/469539+12$30.00

(Hutchinson 1999). They also form part of a systematic experimental study to find the effect of ion size on the structure of molten trivalent metal halides and related compounds (Wasse and Salmon 1998a, b, 1999a, b, c, Wasse *et al* 2000).

All of the chosen tribromide salts have similar physical properties (table 1) which indicate isomorphism in the liquid state. For example, the cation radii (Shannon 1976) and Pettifor (1986) chemical parameters are comparable and the systems all crystallize into the same hexagonal close-packed $FeCl_3$-type structure at room temperature, wherein the cation is octahedrally coordinated by anions (Brown *et al* 1968, Müller 1993). In the case of $DyBr_3$ and YBr_3 this is particularly helpful since the cation coherent neutron scattering lengths are significantly different (Sears 1992). Hence it is possible to simplify the complexity of correlations associated with a single neutron diffraction measurement by the application of difference function methods (Wasse and Salmon 1999a).

Table 1. The radius r_M for sixfold-coordinated cations (Shannon 1976), room temperature crystal structure, molar volume V_{RT} (Brown *et al* 1968), cation Pettifor (1986) chemical parameter χ_M and melting point temperature T_m (Brown 1968) of several MBr_3 systems.

Salt	r_M (Å)	Crystal structure	V_{RT} (cm^3 mol^{-1})	χ_M	T_m (°C)
$DyBr_3$	0.91	$FeCl_3$	84.07	0.685	879
YBr_3	0.90	$FeCl_3$	83.22	0.66	913
$HoBr_3$	0.90	$FeCl_3$	83.22	0.6825	919
$ErBr_3$	0.89	$FeCl_3$	82.56	0.68	923

2. Theory

In a neutron diffraction experiment on a molten MBr_3 salt comprising paramagnetic cations the differential scattering cross-section per ion for unpolarized neutrons can be written as

$$\left(\frac{d\sigma}{d\Omega}\right)_{tot} = \left(\frac{d\sigma}{d\Omega}\right)_{mag} + \left(\frac{d\sigma}{d\Omega}\right)_{nucl}. \tag{1}$$

For the present materials, the rare-earth cations Dy^{3+}, Ho^{3+} and Er^{3+} exhibit paramagnetism and in the free-ion approximation their paramagnetic differential scattering cross-section $(d\sigma/d\Omega)_{mag}$ can be calculated by using the scheme outlined by Wasse and Salmon (1999a). In general, the coherent scattering length of an ion of chemical species α is complex and can be represented as $b_{coh,\alpha} = b_\alpha + ib'_\alpha$ whence the nuclear differential scattering cross-section is given by

$$\left(\frac{d\sigma}{d\Omega}\right)_{nucl} = F(k) + \sum_\alpha c_\alpha(|b_{coh,\alpha}|^2 + |b_{inc,\alpha}|^2)[1 + P_\alpha(k)] \tag{2}$$

where c_α, $b_{inc,\alpha}$ and $P_\alpha(k)$ are the atomic fraction, incoherent scattering length and inelasticity correction (Yarnell *et al* 1973, Howe *et al* 1989) for chemical species α and k is the magnitude of the scattering vector. The total structure factor is defined by

$$F(k) = A[S_{MM}(k) - 1] + B[S_{MBr}(k) - 1] + C[S_{BrBr}(k) - 1] \tag{3}$$

where $S_{\alpha\beta}(k)$ is a Faber–Ziman partial structure factor and the coefficients are

$$A = c_M^2(b_M^2 + b_M'^2) \qquad B = 2c_M c_{Br}(b_M b_{Br} + b'_M b'_{Br}) \qquad C = c_{Br}^2(b_{Br}^2 + b_{Br}'^2).$$

Provided that the diffraction measurements for molten $DyBr_3$ and YBr_3 are made under comparable conditions and the melts can be regarded as isomorphic, subtraction of the structure

factors, $F_{Dy}(k)$ and $F_Y(k)$, gives the first-order difference function

$$\Delta_M(k) \equiv F_{Dy}(k) - F_Y(k) = A'[S_{MM}(k) - 1] + B'[S_{MBr}(k) - 1] \tag{4}$$

which contains only the cation correlations where

$$A' = c_M^2\{(b_{Dy}^2 + b_{Dy}'^2) - (b_Y^2 + b_Y'^2)\}$$

and

$$B' = 2c_M c_{Br}\{b_{Br}(b_{Dy} - b_Y) + b'_{Br}(b'_{Dy} - b'_Y)\}.$$

Forming the difference function $\Delta F'(k)$ can also reduce the complexity of correlations associated with a total structure factor since the M–Br partial structure factor is eliminated, i.e.

$$\begin{aligned}\Delta F'(k) &= F_{Dy}(k) - \frac{b_{Dy}b_{Br} + b'_{Dy}b'_{Br}}{b_{Br}(b_{Dy} - b_Y) + b'_{Br}(b'_{Dy} - b'_Y)}\Delta_M(k) \\ &= C[S_{BrBr}(k) - 1] + D[S_{MM}(k) - 1].\end{aligned} \tag{5}$$

In the case where the imaginary parts of the Y and Br scattering lengths are negligibly small,

$$D = -c_M^2\{b_{Dy}b_Y + b_Y b_{Dy}'^2(b_{Dy} - b_Y)^{-1}\}.$$

The real-space distribution functions $G(r)$, $\Delta G_M(r)$ and $\Delta G'(r)$, corresponding to $F(k)$, $\Delta_M(k)$ and $\Delta F'(k)$ respectively, are obtained from equations (3)–(5) by replacing the $S_{\alpha\beta}(k)$ by the partial pair distribution functions $g_{\alpha\beta}(r)$ whence

$$G(r) = A[g_{MM}(r) - 1] + B[g_{MBr}(r) - 1] + C[g_{BrBr}(r) - 1] \tag{6}$$

$$\Delta G_M(r) = A'[g_{MM}(r) - 1] + B'[g_{MBr}(r) - 1] \tag{7}$$

$$\Delta G'(r) = C[g_{BrBr}(r) - 1] + D[g_{MM}(r) - 1]. \tag{8}$$

The values of the weighting coefficients in equations (3)–(8) are given in table 2 and were calculated using $b_Y = 7.75(2)$ fm, $b_{Ho} = 8.01(8)$ fm and $b_{Br} = 6.795(15)$ fm with negligible imaginary parts (Sears 1992). However, the isotopes ^{164}Dy and ^{167}Er have neutron resonances which make their scattering lengths for thermal neutrons dependent on the incident energy (Lynn and Seeger 1990). At an incident neutron wavelength of 1.798 Å the real and imaginary parts of b_{coh} are 49.4(2) fm and 0.79(1) fm for ^{164}Dy and 3.0(3) fm and 0.183(4) fm for ^{167}Er (Sears 1992). Breit–Wigner theory (Cossy *et al* 1989) was then used to calculate revised scattering lengths for the incident neutron wavelengths of 0.7051 Å and 1.117 Å used for the $DyBr_3$ and $ErBr_3$ experiments respectively. A resonance at −1.88 eV for ^{164}Dy and resonances at 460 meV and 584 meV for ^{167}Er were taken into account (Mughabghab 1984) and real and imaginary parts of 46.3(2) fm and 0.69(1) fm for ^{164}Dy and 2.8(3) fm

Table 2. The weighting coefficients on the $S_{\alpha\beta}(k)$ contributing to the total structure factor $F(k)$ and the difference functions $\Delta_M(k)$ and $\Delta F'(k)$ for the molten tribromide salts.

Salt or isomorphic pair	A (mb)	B (mb)	C (mb)	D (mb)	A' (mb)	B' (mb)
$DyBr_3$	160(4)	408(5)	260(1)	—	—	—
YBr_3	37.5(2)	197.5(7)	260(1)	—	—	—
$(Dy/Y)Br_3$	—	—	260(1)	−78(1)	123(4)	210(5)
$HoBr_3$	40.1(8)	204(2)	260(1)	—	—	—
$ErBr_3$	37.6(2)	197.7(7)	260(1)	—	—	—

and 0.216(4) fm for ^{167}Er were deduced†. The real part of b_{coh} for the other isotopes is tabulated and the imaginary part can be found from the absorption cross-section $\sigma_{abs} = 2\lambda b'$ where λ is the neutron wavelength (Sears 1992). Hence average values of $b_{Dy} = 16.0(2)$ fm, $b'_{Dy} = 0.249(4)$ fm, $b_{Er} = 7.76(16)$ fm and $b'_{Er} = 0.052(1)$ fm were obtained for the elements of natural isotopic abundance.

The mean number of particles of type β contained in a volume defined by two concentric spheres of radii r_i and r_j, centred on a particle of type α, is given by

$$\bar{n}_\alpha^\beta = 4\pi n_0 c_\beta \int_{r_i}^{r_j} r^2 g_{\alpha\beta}(r)\, \mathrm{d}r \tag{9}$$

where n_0 is the ionic number density of the melt.

3. Experimental details

The $DyBr_3$ (99.99%), YBr_3 (99.9+%), $HoBr_3$ (99.99%) and $ErBr_3$ (99.99%) salts, supplied by Aldrich, had a water content of less than 100 ppm and were handled either in high vacuum or under a high-purity argon-gas atmosphere of oxygen and water content both less than 10 ppm. The delivered $DyBr_3$, $HoBr_3$ and $ErBr_3$ salts were finely powdered and had to be pre-melted and re-powdered to increase their packing fraction. The samples were sealed under vacuum in cylindrical silica cells of 5 mm ($DyBr_3$, $HoBr_3$ and $ErBr_3$) or 7 mm (YBr_3) internal diameter and 1 mm wall thickness which had been cleaned using chromic acid and then etched with a 25%-by-mass solution of hydrofluoric acid.

The neutron diffraction experiments were performed using one of three different instruments, namely LAD at the ISIS pulsed neutron source (YBr_3), SLAD at the R2 reactor source of the Studsvik Neutron Research Laboratory, Sweden ($HoBr_3$ and $ErBr_3$), or D4B at the reactor source of the Institut Laue–Langevin in Grenoble, France ($DyBr_3$). Reactor sources were preferred over ISIS for the experiments involving Dy, Ho and Er owing to neutron absorption resonances for these elements at unfavourable energies (Mughabghab 1984). LAD comprises 14 groups of detectors at scattering angles of $\pm5^\circ$, $\pm10^\circ$, $\pm20^\circ$, $\pm35^\circ$, $\pm60^\circ$, $\pm90^\circ$ and $\pm150^\circ$ corresponding to instrumental resolution functions ($\Delta k/k$) of 11%, 6%, 2.8%, 1.7%, 1.2%, 0.8% and 0.5% respectively (Soper *et al* 1989). SLAD comprises several groups of position-sensitive detectors giving a measurement range of $0.3 \leqslant k$ (Å^{-1}) $\leqslant 10.4$ at an incident wavelength of 1.117(1) Å and has a nominal resolution function $\Delta k/k \approx 1\%$ (Wannberg *et al* 1999). D4B comprises two multidetectors giving a measurement range of $0.25 \leqslant k$ (Å^{-1}) $\leqslant 16.5$ at an incident wavelength of 0.7051(7) Å and has a resolution function $\Delta k/k \approx 2\%$ (Ibel 1994).

Each complete experiment comprised the measurement of the diffraction patterns for the samples in their container in a cylindrical vanadium furnace, the empty container in the furnace, the empty furnace and a vanadium rod of diameter comparable to the sample for normalization purposes. The measured intensity for a cadmium neutron-absorbing rod of similar diameter to the sample was also collected for the reactor source experiments to account for the effect of the sample self-shielding on the background count rate at small scattering angles (Bertagnolli *et al* 1976). The LAD and SLAD data analyses were made using the ATLAS (Soper *et al* 1989) and CORRECT (Howe and McGreevy 1995) suite of programs respectively while the D4B analysis followed the scheme given by Salmon (1988). The total paramagnetic scattering cross-section of a cation at the incident neutron wavelength was calculated using the procedure

† Real and imaginary parts of 47.3 fm and 0.83 fm for ^{164}Dy and 3.68 fm and 0.205 fm for ^{167}Er are listed by Lynn and Seeger (1990) at the neutron wavelengths used in the diffraction experiments. Use of these values increases the relevant coefficients in table 2 by $\leqslant$5% but does not otherwise effect the main conclusions of this work.

described by Wasse and Salmon (1999a). The coherent neutron scattering lengths are given in section 2, the neutron absorption cross-section of dysprosium was taken from Goldberg *et al* (1966) and the other scattering length and nuclear cross-section parameters used in the data processing were taken from Sears (1992).

The final $F(k)$ were constructed by merging all those diffraction patterns from the different detector groups that showed good agreement and it was checked that the resultant $F(k)$ tend to the correct high-k limit and obey the usual sum rule relation, and that there is good overall agreement between $F(k)$ and the Fourier back-transform of the corresponding $G(r)$ after the unphysical low-r oscillations have been set to their calculated $G(0)$ limit (Salmon and Benmore 1992).

The temperatures of the $DyBr_3$, YBr_3, $HoBr_3$ and $ErBr_3$ melts were 917(3) °C, 940(3) °C, 950(3) °C and 980(3) °C respectively. The corresponding number densities were calculated using the Tallon–Robinson (1982) relation between the volume change on melting $\Delta V/V_m$ and the entropy change on melting ΔS_m with parameters for trivalent metal halides given by Akdeniz and Tosi (1992), i.e.

$$\Delta S_m/R = 5.0 \ln 2 + 12.4 \Delta V/V_m. \tag{10}$$

In this equation R is the molar gas constant, $\Delta V = V_m - V_{RT}$, V_m is the molar volume of the liquid at the melting point temperature T_m and V_{RT} is the molar volume of the salt at room temperature. For $HoBr_3$, $\Delta S_m = 10.0$ cal K^{-1} mol^{-1} (Dworkin and Bredig 1971) which gives $\Delta V/V_m = 12.6\%$, a value that was also assumed for the other salts. The density at the melting point was then adjusted by a small amount ($\leqslant 1\%$) to that of the experiment using the data of Nisel'son and Lyzlov (1975) to give number densities of 0.0252(6) $Å^{-3}$, 0.0249(5) $Å^{-3}$, 0.0251(6) $Å^{-3}$ and 0.0252(6) $Å^{-3}$ for $HoBr_3$, $DyBr_3$, YBr_3 and $ErBr_3$ respectively. Full experimental details are given by Wasse (1998).

4. Results

On heating $DyBr_3$, YBr_3 and $HoBr_3$ a solid–solid phase transition was observed from the $FeCl_3$-type crystal structure, which is the stable phase at room temperature (Brown *et al* 1968), to a structure having a diffraction pattern resembling that of crystalline YCl_3 (Templeton and Carter 1954). This type of transition with increasing temperature, from a phase in which the anions are hexagonally close packed to a phase where they are cubically close packed, has not previously been reported for these tribromide salts although it has been observed for $ScCl_3$ (Wasse and Salmon 1999b) and $CrCl_3$ (Morosin and Nareth 1964). A comparable transition may also occur for $HoBr_3$ although it was not searched for in the diffraction experiment owing to beam time constraints.

The measured $F(k)$ for molten YBr_3 $HoBr_3$ and $ErBr_3$ (see figure 1) have similar overall features, as anticipated from the expected isomorphism of the liquids and comparable cation coherent scattering lengths. Although $DyBr_3$ is also expected to be isomorphic with the other systems, the measured $F(k)$ for the liquid has a larger magnitude and different features that may be attributed to the much larger cation coherent neutron scattering length. Each function has a prominent first sharp diffraction peak (FSDP), at a position k_{FSDP} of 0.87(2) $Å^{-1}$, 0.82(2) $Å^{-1}$, 0.80(2) $Å^{-1}$ and 0.79(2) $Å^{-1}$ for $DyBr_3$, YBr_3, $HoBr_3$ and $ErBr_3$ respectively, which is a signature of intermediate-range ionic ordering (e.g. Salmon 1994). As for the corresponding trichlorides (Wasse and Salmon 1999c), a small shift of k_{FSDP} to smaller values with decreasing cation radius is observed. The height of the FSDP is largest for $DyBr_3$ which indicates a strong contribution to the FSDP from cation correlations.

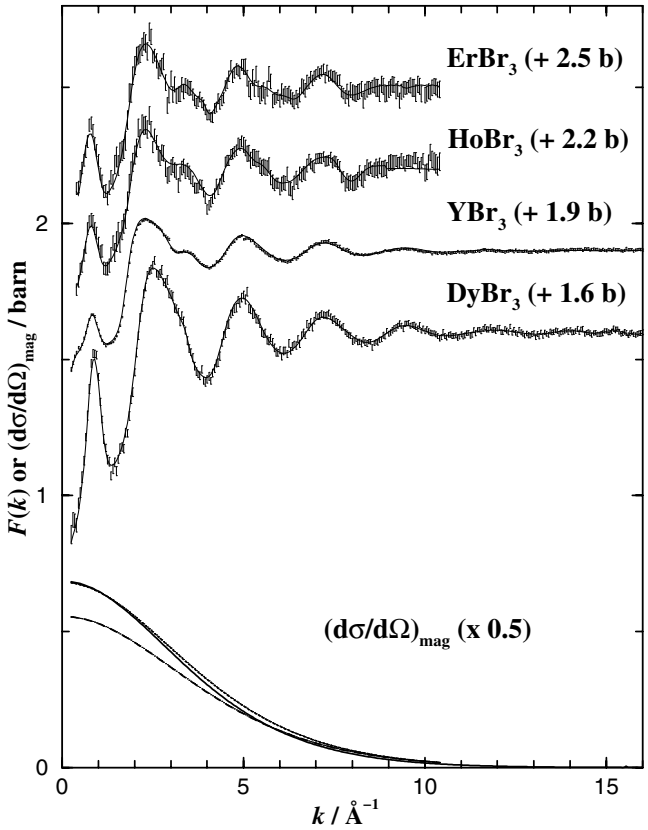

Figure 1. The measured total structure factors $F(k)$ (equation (3)) for molten $DyBr_3$, YBr_3, $HoBr_3$ and $ErBr_3$ at 917(3), 940(3), 950(3) and 980(3) °C respectively. The bars represent the statistical errors on the data points and the solid curves are the Fourier back-transforms of the corresponding $G(r)$ given by the solid curves in figure 2. The calculated paramagnetic scattering cross-sections $(d\sigma/d\Omega)_{mag}$ for Dy^{3+}, Ho^{3+} and Er^{3+} (see equation (1)), scaled by a factor of 0.5, are also shown and are denoted by the solid, dotted and dashed curves respectively.

The total pair distribution functions are shown in figure 2. The first peak may be identified with nearest-neighbour M–Br correlations by comparison with the room and high-temperature crystal structures and the sum of radii of the cation (table 1) and bromide ion (1.96 Å, Shannon 1976). Integrating over the first peak to the first minimum in $G(r)$ gives $\bar{n}_M^{Br} \approx 6$. The second peaks will, by comparison with the crystal structures, have a strong contribution from the Br–Br correlations and, accordingly, the ratio of the first to second peak heights is larger for $DyBr_3$ than for the other salts that have much smaller cation coherent scattering lengths. For example, the B:C ratio in equation (3) is 1.569 for $DyBr_3$ and 0.760 for YBr_3.

The first-order difference function $\Delta_M(k)$ obtained for the $(Dy/Y)Br_3$ system on the assumption of isomorphism is shown in figure 3. It was obtained by combining the $F(k)$ for molten $DyBr_3$ and YBr_3 that were measured using different instruments, namely D4B and LAD respectively. However, the peaks in the measured diffraction patterns are relatively broad and the resolution functions are roughly comparable, i.e. $\Delta k/k \approx 2\%$ for D4B at an incident wavelength of 0.7 Å and $\Delta k/k = 0.8$–2.8% for the main LAD detector groups used to construct the total structure factor. Furthermore, the difference function is well behaved,

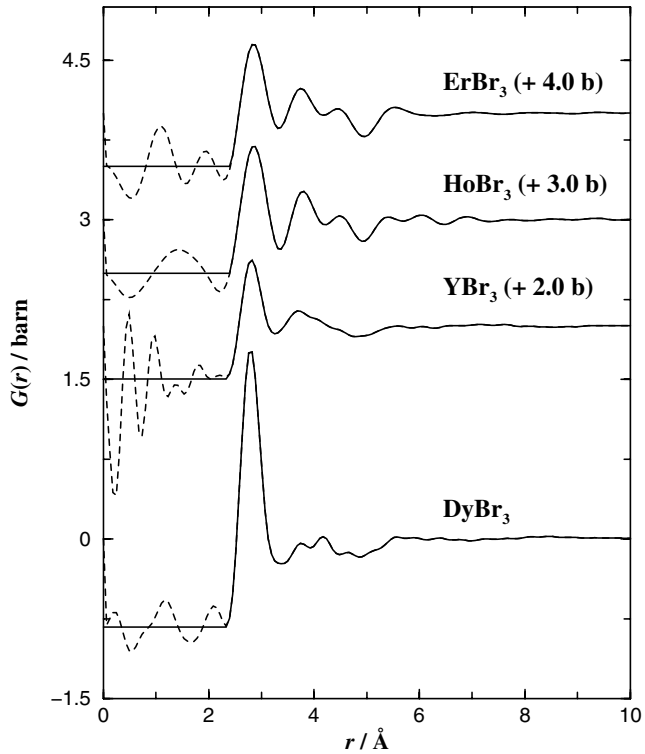

Figure 2. The total pair distribution functions $G(r)$ (equation (6)) for molten $DyBr_3$, YBr_3, $HoBr_3$ and $ErBr_3$ obtained by Fourier transforming the $F(k)$ given by the error bars in figure 1. The unphysical low-r oscillations about the $G(0)$ limits are shown by the broken curves.

i.e. the unphysical low-r features in the corresponding real-space function oscillate about the correct $\Delta G_M(0)$ limit (figure 4) and there is good overall agreement between $\Delta_M(k)$ and the Fourier back-transform of $\Delta G_M(r)$ after these low-r features are set to $\Delta G_M(0)$ (Salmon and Benmore 1992).

The first-order difference function has a strong FSDP at $k_{FSDP} = 0.92(2)$ Å^{-1}, which must arise from cation correlations, and strong oscillations extending up to 16 Å^{-1}. There is a correspondingly strong first peak in $\Delta G_M(r)$ at a distance $r_{MBr} = 2.78(2)$ Å that is asymmetric and identified with nearest-neighbour M–Br correlations. Integrating over this peak to the first shoulder at 3.25(2) Å gives a coordination number $\bar{n}_M^{Br} = 5.8(2)$ while integrating to the first minimum at 3.62(2) Å gives $\bar{n}_M^{Br} = 6.4(2)$. Hence the cation is approximately sixfold coordinated by an asymmetric distribution of anions. The second peak in $\Delta G_M(r)$ at 4.22(2) Å may be assigned to nearest-neighbour M–M correlations since $g_{MM}(r)$ is strongly weighted in equation (7) and the distance falls in an appropriate range. The same peak is also visible in the total pair distribution function $G(r)$ for molten $DyBr_3$ at 4.21(2) Å where $g_{MM}(r)$ is also given a relatively large weight (table 2). For perfect MBr_6^{3-} octahedra the M–M distance is $2r_{MBr} = 5.56(4)$ Å if the polyhedra are vertex-sharing with a linear M–Br–M bond while it is $\sqrt{2}r_{MBr} = 3.93(3)$ Å if the polyhedra are edge-sharing with nearest-neighbour M^{3+} ions lying in the same plane. The appearance of a distinct peak at a relatively short M–M distance therefore suggests that a substantial number of the MBr_6^{3-} octahedra in liquid $(Dy/Y)Br_3$ are edge-sharing.

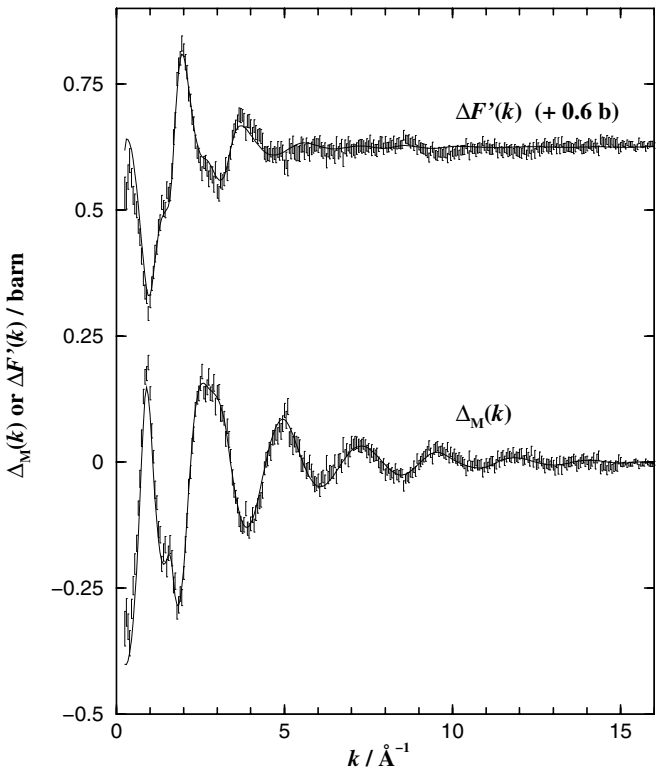

Figure 3. The measured difference functions $\Delta_M(k)$ (equation (4)) and $\Delta F'(k)$ (equation (5)) derived from the $DyBr_3$ and YBr_3 total structure factors of figure 1. The bars represent the statistical errors on the data points and the solid curves are the Fourier back-transforms of the corresponding $\Delta G_M(r)$ and $\Delta G'(r)$ functions given by the solid curves in figure 4.

The difference function $\Delta F'(k)$ is shown in figure 3. It is well behaved, i.e. the unphysical low-r features in the corresponding real-space function oscillate about the correct $\Delta G'(0)$ limit (figure 4) and there is good overall agreement between $\Delta F'(k)$ and the Fourier back-transform of $\Delta G'(r)$ after these low-r features are set to $\Delta G'(0)$ (Salmon and Benmore 1992). $\Delta F'(k)$ has a marked negative-going FSDP at 0.93(2) Å^{-1} which is consistent with there being a FSDP in $S_{MM}(k)$ since this partial structure factor is given a large negative weighting in equation (5). The first broad asymmetric peak in $\Delta G'(r)$ at the position $r_{BrBr} = 3.69(3)$ Å (figure 4) will be dominated by Br–Br correlations by comparison with the room and high-temperature crystal structures. Its integration over the range $2.88(2) \leqslant r$ (Å) $\leqslant 4.79(2)$ gives a minimum coordination number $\bar{n}_{Br}^{Br} = 7.5(2)$ on assuming that the M–M correlations are negligibly small. However, the M–M correlations are given a negative weighting in equation (8) such that if a coordination number $\bar{n}_{M}^{M} = 3$ is assumed, as in both the low- and high-temperature crystal structures, then an increased value of $\bar{n}_{Br}^{Br} = 10.2(2)$ is obtained.

5. Discussion

The assumption of isomorphism for $DyBr_3$ and YBr_3 is supported by the present diffraction work. For example, the same solid-state phase transition with increasing temperature was observed for both systems, comparable nearest-neighbour parameters for the liquid state were

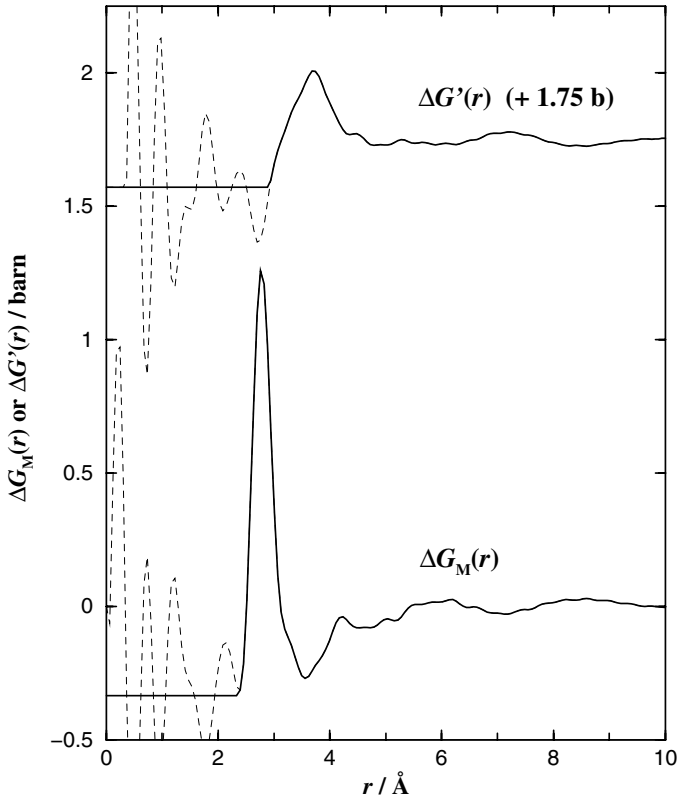

Figure 4. The real-space difference functions $\Delta G_{\mathrm{M}}(r)$ (equation (7)) and $\Delta G'(r)$ (equation (8)) for the (Dy/Y)Br_3 isomorphic pair obtained by Fourier transforming the corresponding k-space functions given by the error bars in figure 3. The unphysical low-r oscillations about the $\Delta G_{\mathrm{M}}(0)$ and $\Delta G'(0)$ limits are shown by the broken curves.

obtained from the total pair distribution functions (table 3) and the combination of the total structure factors gives rise to well behaved difference functions. Strong similarities are also found with the structures of $HoBr_3$ and $ErBr_3$. For example, the same solid-state phase transition was observed for $HoBr_3$, the $F(k)$ functions measured for YBr_3, $HoBr_3$ and $ErBr_3$, which have cations with similar coherent scattering lengths, are alike and the nearest-neighbour parameters obtained from the corresponding $G(r)$ functions (table 3) are comparable. The FSDPs in the measured reciprocal-space functions are consistent with intermediate-range ionic ordering of the cation correlations with a periodicity $2\pi/k_{\mathrm{FSDP}}$ in the range 7–8 Å (Salmon 1994).

The data for all four systems are consistent with the survival on melting of a substantial number of the MBr_6^{3-} octahedral motifs that are characteristic of both the room and high-temperature crystalline phases. The ratio of the nearest-neighbour peak positions r_{BrBr}:r_{MBr} is in the range 1.32–1.35, suggesting a distortion from regular octahedral geometry for which the ratio is $\sqrt{2}$, and the appearance in $\Delta G_{\mathrm{M}}(r)$ of a distinct peak at a relatively short M–M nearest-neighbour distance suggests that a large number of these octahedra are edge-sharing. In molten YBr_3 the presence of distorted edge-sharing YBr_6^{3-} octahedra is supported by Raman spectroscopy experiments (Dracopoulos *et al* 1997). Furthermore, distorted edge-sharing octahedra also feature in the liquid phases of $DyCl_3$, YCl_3, $HoCl_3$ and $ErCl_3$ which are systems

Table 3. The local coordination environment of the ions in the molten tribromide salts.

Salt	Function	r_{MBr} (Å)	Integration range† (Å)	$\bar{n}_M^{Br}$	r_{BrBr} (Å)	r_{BrBr}/r_{MBr}
$DyBr_3$	$G(r)$	2.79(2)	2.33(2)–3.33(2)[a]	6.1(2)	3.76(2)	1.35(1)
YBr_3	$G(r)$	2.81(2)	2.33(2)–3.25(2)[a]	6.0(2)	3.70(2)	1.32(1)
$(Dy/Y)Br_3$	$\Delta G_M(r)$	2.78(2)	2.33(2)–3.62(2)[a]	6.4(2)	—	—
		2.78(2)	2.33(2)–3.25(2)[b]	5.8(2)	—	—
	$\Delta G'(r)$	—	—	—	3.69(3)	1.33(1)
$HoBr_3$	$G(r)$	2.86(2)	2.39(2)–3.37(2)[a]	6.4(2)	3.79(2)	1.33(1)
$ErBr_3$	$G(r)$	2.85(2)	2.39(2)–3.31(2)[a]	6.5(2)	3.75(2)	1.32(1)

† Integrating to (a) the first minimum or (b) the first shoulder in the real-space function.

that also melt from the YCl_3-type crystal structure (Papatheodorou 1977, Wasse and Salmon 1999c, Takagi *et al* 1999, Wasse *et al* 2000). The measured $\Delta G'(r)$ difference function shows a large reduction in $\bar{n}_{Br}^{Br}$ on melting from 12 (Templeton and Carter 1954) to between 7.4 and 10. A reduction on melting of the anion–anion coordination number from 12 to between 8 and 10 is also reported for YCl_3 (Saboungi *et al* 1991, Wasse and Salmon 1999c).

Since the first peaks in $\Delta G_M(r)$ and $\Delta G'(r)$ are identified with M–Br and Br–Br correlations respectively, it is instructive to compare the functions

$$[\Delta G_M(r) - \Delta G_M(0)]/B' = g_{MBr}(r) + E g_{MM}(r) \tag{11}$$

and

$$\left[\Delta G'(r) - \Delta G'(0)\right]/C = g_{BrBr}(r) + F g_{MM}(r) \tag{12}$$

for those isomorphic pairs, $(Dy/Y)Br_3$ and $(La/Ce)Br_3$ (Wasse and Salmon 1999a), for which diffraction data are available. The cation radius increases from 0.91 Å for Dy^{3+} and Y^{3+} to 1.02 Å for La^{3+} and Ce^{3+} (Shannon 1976) and the tribromides of the latter crystallize in the UCl_3-type structure at room temperature wherein the cation is ninefold coordinated by anions (Zachariasen 1948, Taylor and Wilson 1974). In equation (11), La replaces Dy and Ce replaces Y in the definition of B' for the $(La/Ce)Br_3$ isomorphic pair while E and F are 0.586(24) and −0.300(4) for $(Dy/Y)Br_3$ or 0.320(6) and −0.0958(9) for $(La/Ce)Br_3$. The functions, plotted in figure 5, both show an asymmetric distribution of anions around the cation with a similar degree of penetration of $g_{BrBr}(r)$ into the first peak of $g_{MBr}(r)$. This penetration decreases with cation radius, as shown by the neutron diffraction results for $AlBr_3$ and $GaBr_3$, in keeping with a trend towards more molecular-type structures for which $\bar{n}_M^{Br} = 4.0(2)$ (Saboungi *et al* 1993, Akdeniz *et al* 1998). The M–Br coordination number does not change significantly from six when $(Dy/Y)Br_3$ melts and $r_{BrBr}/r_{MBr} = 1.33(1)$ in the liquid whereas $(La/Ce)Br_3$ undergoes a reduction of the M–Br coordination number from 9 to 7.4(2) on melting and $r_{BrBr}/r_{MBr} = 1.25(2)$ in the melt. The same distance ratio for molten $LaBr_3$ is obtained from x-ray diffraction experiments although a reduced M–Br coordination number of six is reported albeit from a total pair distribution function in which there is considerable overlap of the $g_{\alpha\beta}(r)$ (Okamoto and Ogawa 1999).

6. Conclusions

On heating $DyBr_3$, YBr_3 and $HoBr_3$ a solid–solid phase transition was observed from the $FeCl_3$-type crystal structure to possibly the YCl_3-type crystal structure. A corresponding transition was not searched for in the case of $ErBr_3$ but may be anticipated on the basis of the similar physico-chemical properties of all four systems. The molten phases of $DyBr_3$, YBr_3,

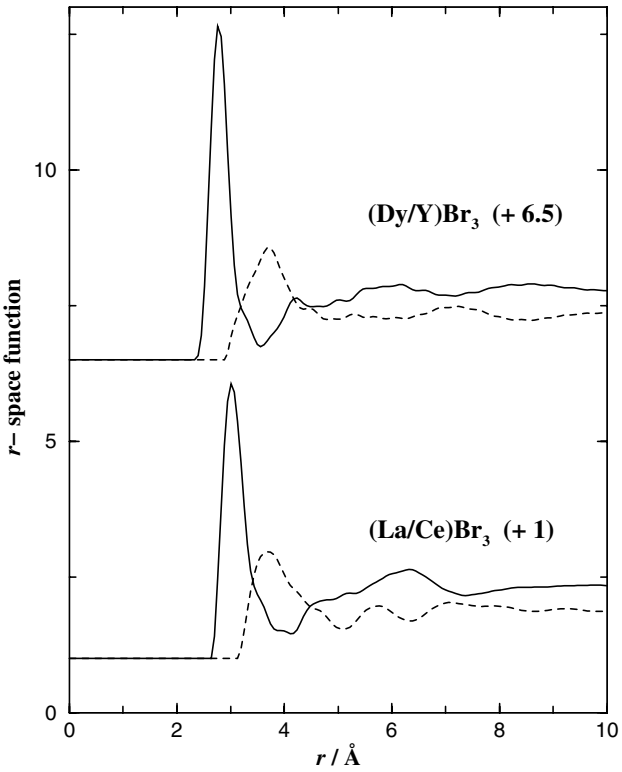

Figure 5. The real-space difference functions $[\Delta G_{\mathrm{M}}(r) - \Delta G_{\mathrm{M}}(0)]/B'$ (solid curves) and $[\Delta G'(r) - \Delta G'(0)]/C$ (broken curves) for the molten $(Dy/Y)Br_3$ and $(La/Ce)Br_3$ isomorphic pairs defined by equations (11) and (12) respectively.

$HoBr_3$ and $ErBr_3$ are found to comprise distorted MBr_6^{3-} octahedral motifs, many of which are edge-sharing, which connect to give intermediate-range ordering of the cation correlations as manifested by the appearance of a first sharp diffraction peak.

Acknowledgments

It is a pleasure to thank Paul Madden for his encouragement of the present work, Francis Hutchinson, Moises Silbert and Mark Wilson for useful discussions on MX_3 systems, Chris Anson for help with the crystal structures and the EPSRC and EC TMR-LSF for financial support. It is also a pleasure to thank Spencer Howells, Chris Benmore, John Dreyer and Duncan Francis at ISIS, Bertil Trostell, Anders Wannberg and Robert McGreevy at Studsvik, Ingrid Petri at Bath and Henry Fischer at the ILL for their help with the neutron diffraction experiments.

References

Akdeniz Z, Price D L, Saboungi M-L and Tosi M P 1998 *Plasmas Ions* **1** 3
Akdeniz Z and Tosi M P 1992 *Proc. R. Soc.* A **437** 85
Bertagnolli H, Chieux P and Zeidler M D 1976 *Mol. Phys.* **32** 759
Brown D 1968 *Halides of the Lanthanides and Actinides* (London: Wiley)

Brown D, Fletcher S and Holah D G 1968 *J. Chem. Soc.* A 1889
Cossy C, Barnes A C, Enderby J E and Merbach A E 1989 *J. Chem. Phys.* **90** 3254
Dracopoulos V, Gilbert B, Børrensen B, Photiadis G M and Papatheodorou G N 1997 *J. Chem. Soc., Faraday Trans.* **93** 3081
Dworkin A S and Bredig M A 1971 *High Temp. Sci.* **3** 81
Goldberg M D, Mughabghab S F, Purohit S N, Magurno B A and May V M 1966 *Neutron Cross Sections* BNL 325 vol IIC, 2nd edn (Brookhaven, NY: Brookhaven National Laboratory)
Howe M A and McGreevy R L 1995 *Studsvik Neutron Research Laboratory Internal Report* Version 2.18 (NFL, Studsvik, Sweden)
Howe M A, McGreevy R L and Howells W S 1989 *J. Phys.: Condens. Matter* **1** 3433
Hutchinson F 1999 *DPhil Thesis* University of Oxford, UK
Hutchinson F, Rowley A J, Walters M K, Wilson M, Madden P A, Wasse J C and Salmon P S 1999 *J. Chem. Phys.* **111** 2028
Ibel K 1994 *The Yellow Book—Guide to Neutron Research Facilities at the ILL* (Grenoble: ILL)
Lynn J E and Seeger P A 1990 *At. Data Nucl. Data Tables* **44** 191
Madden P A and Wilson M 1996 *Chem. Soc. Rev.* **25** 339
Morosin B and Nareth A 1964 *J. Chem. Phys.* **40** 1958
Mughabghab S F 1984 *Neutron Cross Sections* Part B, vol 1 (Orlando, FL: Academic)
Müller U 1993 *Inorganic Structural Chemistry* (Chichester: Wiley)
Nisel'son L A and Lyzlov Yu N 1975 *Dokl. Akad. Nauk SSSR* **220** 608
Okamoto Y and Ogawa T 1999 *Z. Naturf.* a **54** 91
Papatheodorou G N 1977 *J. Chem. Phys.* **66** 2893
Pettifor D G 1986 *J. Phys. C: Solid State Phys.* **19** 285
Saboungi M-L, Howe M A and Price D L 1993 *Mol. Phys.* **79** 847
Saboungi M-L, Price D L, Scamehorn C and Tosi M P 1991 *Europhys. Lett.* **15** 283
Salmon P S 1988 *J. Phys. F: Met. Phys.* **18** 2345
Salmon P S 1994 *Proc. R. Soc.* A **445** 351
Salmon P S and Benmore C J 1992 *Recent Developments in the Physics of Fluids* ed W S Howells and A K Soper (Bristol: Hilger) p F225
Sears V F 1992 *Neutron News* **3** 26
Shannon R D 1976 *Acta Crystallogr.* A **32** 751
Soper A K, Howells W S and Hannon A C 1989 *Rutherford Appleton Laboratory Report* RAL-89-046
Takagi R, Hutchinson F, Madden P A, Adya A K and Gaune-Escard M 1999 *J. Phys.: Condens. Matter* **11** 645
Tallon J L and Robinson W H 1982 *Phys. Lett.* A **87** 365
Taylor J C and Wilson P W 1974 *Acta Crystallogr.* B **30** 2803
Templeton D H and Carter G F 1954 *J. Phys. Chem.* **58** 940
Wannberg A, Mellergård A, Zetterström P, Delaplane R G, Grönros M, Karlsson K-E and McGreevy R L 1999 *J. Neutron Res.* **8** 133
Wasse J C 1998 *PhD Thesis* University of East Anglia, UK
Wasse J C and Salmon P S 1998a *Physica* B **241–243** 967
Wasse J C and Salmon P S 1998b *J. Phys.: Condens. Matter* **10** 8139
Wasse J C and Salmon P S 1999a *J. Phys.: Condens. Matter* **11** 1381
Wasse J C and Salmon P S 1999b *J. Phys.: Condens. Matter* **11** 2171
Wasse J C and Salmon P S 1999c *J. Phys.: Condens. Matter* **11** 9293
Wasse J C, Salmon P S and Delaplane R G 2000 *Physica* B **276–278** 433
Yarnell J L, Katz M J, Wenzel R G and Koenig S H 1973 *Phys. Rev.* A **7** 2130
Zachariasen W H 1948 *Acta Crystallogr.* **1** 265